# Picosecond photoemission probing of integrated circuits: Capabilities, limitations, and applications

by R. Clauberg H. Beha A. Blacha H. K. Seitz

The capabilities and limitations of the novel photoemission probing technique for signal measurements on internal nodes of VLSI integrated circuits are reviewed with respect to the range of possible applications of this method. Aspects such as voltage sensitivity, time resolution, minimum accessible feature size, sensitivity to perturbation effects, and impact on the circuit under test are considered. It is concluded that the especially high voltage sensitivity of this new method opens the field of diagnostics of circuits with ultrafast devices but partly low signal repetition rates, which is not accessible by other means. Such chips include. for example, complex logic chips and special telecommunication chips.

<sup>®</sup>Copyright 1990 by International Business Machines Corporation. Copying in printed form for private use is permitted without payment of royalty provided that (1) each reproduction is done without alteration and (2) the *Journal* reference and IBM copyright notice are included on the first page. The title and abstract, but no other portions, of this paper may be copied or distributed royalty free without further permission by computer-based and other information-service systems. Permission to *republish* any other portion of this paper must be obtained from the Editor.

## 1. Introduction

In recent years, the growing complexity of integrated circuits and their ever-faster working speed have led to the need for contactless measurement methods for logicstate analysis and waveform measurements on internal nodes of very-large-scale integration (VLSI) circuits. An important requirement to be fulfilled in this environment is the capability of measuring ultrafast signals with rise and fall times below 10 ps on metal lines of  $0.5-1.0-\mu m$ width and spacing with a voltage resolution better than 5 mV. In addition, it is desirable that the diagnostic technique be applicable to all technologies, rather than being limited to Si- or GaAs-based circuitry only. For single devices and common circuits, electron-beam sampling [1-3] is a well-established probing method which has even demonstrated the capability of measuring entire signals rising in less than 10 ps within only seven seconds [4, 5] on submicron lines. But these results have been achieved with pulse repetition rates of a few gigahertz, which may not be available at arbitrary nodes in a VLSI circuit. With repetition rates of 1 MHz or less, the measurement time for electron-beam sampling of picosecond signals increases tremendously. For signals rising on the femtosecond time scale on GaAs circuits,

electro-optical sampling (EOS) has demonstrated its applicability [6, 7]. However, EOS is limited in spatial resolution and by its sensitivity to crosstalk effects [8], especially in its extensions toward application to Si-based circuits.

Under the conditions for contactless testing of future high-speed VLSI circuits, the voltage sensitivity of the applied measurement method becomes a crucial parameter. In addition, situations in which the voltage sensitivity of electron-beam probing is no longer sufficient for the desired testing application are already foreseeable in the near future. For this range of applications, a new method with an especially high voltage sensitivity is needed. A technique which offers the required capabilities is the newly developed method of photoemission probing [9-19]. Theoretical analyses have shown that signals can be measured with a resolution of a few picoseconds [20-22], and that a voltage sensitivity of about 0.6 V per pulse for pulses of 1 ps focused to a 0.5-µm spot size is achievable [23]—a value which clearly outperforms that for electron-beam sampling with picosecond pulses.

In this paper we summarize the already demonstrated capabilities of photoemission probing, as well as its limitations, and describe the range of applications where the special features of this method offer advantages over other contactless testing methods.

# 2. Basic principle

In photoemission probing, a continuous (real-time mode) or pulsed (stroboscopic sampling mode) laser beam is focused onto a metal line to induce photoemission of electrons from the metal. For this purpose, the energy transferred to the electrons must exceed the work function of the metal to allow the ejection of the electron through the metal surface into vacuum. The absorption of the incident light may occur either in a single-photon process, where the necessary energy is provided by a single photon, or in a multi-photon process, where this energy is provided by n photons which transfer their energies to the electron in a fast succession of excitation steps. The important parameters for photoemission probing are the total yield of emitted electrons and the width of the energy distribution, both of which determine the voltage sensitivity of photoemission probing. In the case of an n-photon process, the electron is emitted with a kinetic energy equal to

$$E_{\rm k} = nh\nu - (\Phi + E_{\rm h}),\tag{1}$$

where  $h\nu$  is the photon energy,  $\Phi$  the work function, i.e., the height of the surface barrier, and  $E_{\rm b}$  the binding energy of the electron with respect to the Fermi energy. The width of the distribution of kinetic energies ranges from  $\Delta E = 0$  for electrons of binding energy  $E_{\rm b} = nh\nu - \Phi$  up to

$$\Delta E = nh\nu - \Phi \tag{2}$$

for electrons at the Fermi level. The width  $\Delta E$  of the energy distribution is given by the photon energy chosen, the kind of excitation process  $(n=1,2,3,\cdots)$ , and the work function  $\Phi$  of the material. For photoemission into vacuum, work functions of clean metals range from 2.4 eV for lithium to 5.3 eV for platinum [24]. For air-exposed metals, the work function is often considerably reduced, leading to values around 4 eV for most commonly used metals.

The total yield of the photoemission process is obtained by integrating the photoelectron distribution Y(E) over the entire range of kinetic energies from zero to  $nh\nu - \Phi$ ,

$$Y_{\text{total}} = \int_0^{nh\nu - \Phi} Y(E) \ dE. \tag{3}$$

For energy distributions with width 1 to 2 eV, the total yield in the single-photon process from, e.g., atomically clean metals is of the order of  $10^{-4}$  electrons per incident photon [25]. This value decreases to about  $10^{-6}$  electrons per incident photon for air-exposed aluminum, according to our own results [9].

For the multi-photon process, total yields of  $8 \times 10^{-11}$  electrons per photon have been obtained in a three-photon excitation with a photon intensity of 500 MW/cm<sup>2</sup> on a gold surface [12]. The general observation is that very high photon intensities are needed in a multi-photon process to obtain photo-yields comparable to that of the single-photon process. Also, problems of device impact by visible light have been observed. Therefore, we restrict the remainder of this paper to the single-photon process.

The voltage level at the point from which electron emission occurs is determined by accelerating the electrons toward a reference or retarding field electrode. If the reference electrode has the same potential as the point of electron emission on the integrated circuit, all photoemitted electrons pass the reference electrode and are guided toward an electron detector. In the case of a positive voltage, i.e., when the potential at the retarding electrode is larger than at the point under test, all the (negatively charged) electrons reach the detector, and the detected current is maximal. When a change is made to negative voltages, a potential barrier appears between the sample and the reference electrode, which decreases the detected electron current. For a potential difference larger than the maximum kinetic energy  $\Delta E$  of the emitted electrons, the detected current vanishes. Hence, the detected electron current is a function of the potential difference between the point of the sample being tested and the reference or retarding electrode. The voltage change can then be extracted by calibrating the change in

the intensity of measured electrons against the change in voltage, or it can be extracted directly by using a feedback loop to keep the measured intensity constant by shifting the retarding voltage. The latter approach exploits the fact that the relative shift in energy is determined only by the difference between the voltage at the sample and the retarding voltage; i.e., each change at the sample can be compensated by a corresponding change at the retarding electrode.

In the real-time mode, the voltage change is detected directly, and the possible time resolution of the measurement is determined by the reaction time of the electron detector, which counts the number of electrons passing the retarding field barrier, and the possible timespread of the electrons during transport toward the detector due to various start energies. If a feedback loop is used, the time resolution is further limited by the total time it takes the emitted electrons to travel the distance between the retarding field electrode and the detector plus the time needed to adjust the correct retarding voltage. For very fast signals, this approach is no longer sufficient, and the sampling mode must be applied to detect voltage changes on the picosecond time scale. Here, picosecond laser pulses are used to induce photoemission. The time resolution is no longer achieved by directly measuring the time dependence of the photoemission signal, but by measuring the photoemission signal as a function of the delay between the signal on the device and the laser pulse which excites the electrons into vacuum. This method works only for periodic signals and requires a synchronization of the signal at the device with the probing laser pulse. For each delay selected, the voltage level is measured just as if there were a constant signal voltage at the device; i.e., the detector only determines the intensity of electrons which pass the retarding field barrier. A time-spread in the pulse reaching the detector does not influence the measurement as long as the delay is changed on a much larger time scale. The entire signal waveform is then determined by combining all the snapshot pictures for different delay times. The time resolution of the sampling mode is determined by the time the induced pulse of emitted electrons interacts with the electric potential of the sample, hence the duration of the laser pulse, the time scale of the photoemission process, and the time in which the emitted electrons still react to voltage changes at the sample. Details are discussed in the subsection on time resolution.

## 3. Capabilities and limits

For a novel contactless diagnostic method such as photoemission probing, the most important question concerns the capabilities and limits of the method in comparison with those of established techniques.

Considering signal measurements at internal nodes of integrated circuits, the key parameters of any probing method are voltage sensitivity, time resolution, minimum accessible feature size, sensitivity to perturbation effects, and impact on the circuit under test. In the following we summarize these parameters for photoemission probing and point out the main physical effects which determine the related limits.

## Voltage sensitivity

The voltage sensitivity of a method is determined by the various noise sources which disturb the signal. Such noise sources are, for example, shot noise in the electron or photon detector, thermal noise in the electronic components, laser noise, and electromagnetic stray fields from the environment. Practically all noise sources except shot noise can be reduced by engineering means. Therefore, we consider only the contributions from shot noise in the following and assume that other noise contributions can be reduced below the shot-noise value.

For a retarding field voltage detector which counts all the electrons with energies between the operation energy  $E_0$  of the detector and a certain cutoff energy  $E_1$ , the minimum resolvable voltage is determined [23] by

$$\Delta V = \frac{1}{\sqrt{N_{\text{prim}} Y_{\text{total}} \eta_D}} S(E_0, E_1) K_{\text{conf}}, \tag{4}$$

where the shape factor

$$S(E_0, E_1) = \frac{\sqrt{\int_{E_0}^{E_1} y(E) dE}}{\{e[y(E_0) - y(E_1)]\}}$$
 (5)

depends only on the energy distribution y(E) of the electron yield normalized to

$$\int_0^\infty y(E) \ dE = 1. \tag{6}$$

 $N_{\rm prim}$  is the number of incident primary particles in the signal integration time,  $Y_{\rm total}$  the total electron yield per incident primary particle, and the confidence factor  $K_{\rm conf}$  determines the statistical error of  $\Delta V$ .  $K_{\rm conf}=1$  means that a measured voltage is within the interval  $[V-\Delta V,V+\Delta V]$  with a probability of 66%. The usual requirement is  $K_{\rm conf}=3$ , which means that this probability is 96%.  $\eta_{\rm D}$  gives the detector efficiency with respect to electrons having energies between  $E_0$  and  $E_1$ . It is clear from Equation (4) that the voltage resolution is determined by the number of electrons which reach the detector in the signal integration time  $\tau$ , i.e., by  $N_{\rm prim} Y_{\rm total} \eta_{\rm D}$ , and by the shape factor S of the energy distribution of the emitted electrons. The first factor should be as large as possible and the latter as small as

175

possible to achieve the best voltage resolution  $\Delta V$ . For a pulsed excitation beam,  $N_{\rm prim}$  is given as  $N_{\rm prim}=N_{\rm prim}^{\rm pulse}R\tau$ , where  $N_{\rm prim}^{\rm pulse}$  is the number of primary particles per pulse, R the pulse-repetition rate, and  $\tau$  the signal-integration time over which the signal is summed to achieve the desired voltage resolution. Accordingly, the number of emitted electrons per pulse is  $N_{\rm el}^{\rm pulse} = N_{\rm prim}^{\rm pulse} Y_{\rm total}$ . Hence, if the pulse-repetition rate R is fixed, the best voltage sensitivity should be achieved with the largest possible number of emitted electrons per pulse without causing damage from the correspondingly large incident primary beam. However, this is not true, because a high electron density in a pulse leads to a broadening of the energy distribution of the emitted electrons and therefore to an enhanced shape factor. For threshold photoemission, as used in photoemission probing, the shape factor is proportional to the width  $\Delta E$  of the energy distribution. and the energy broadening caused by the Coulomb repulsion of the electrons leads [23] to

$$\Delta E = \Delta E_0 + \beta N_{\rm el}^{\rm pulse} \,, \tag{7}$$

where  $\Delta E_0$  is the width of the energy distribution without the Coulomb broadening and  $\beta$  is the proportionality constant which describes the linear increase of the Coulomb broadening with electron density. This results in an optimum voltage resolution  $\Delta V$  when the number of emitted electrons per pulse is

$$N_{\rm el}^{\rm pulse}({\rm optimum}) = \Delta E_0/\beta.$$
 (8)

Experimental analyses of photoemission probing with laser beams of Gaussian intensity distribution and pulses of 1–2 ps lead to  $N_{\rm el}^{\rm pulse}$  (optimum) = 200 electrons per pulse if 50% of the electrons are emitted from a circle of 1.5- $\mu$ m diameter and 55 electrons per pulse if emitted from a circle of 0.5- $\mu$ m diameter [23]. The corresponding voltage resolution for the 0.5- $\mu$ m-diameter spot is

$$\Delta V = 0.6 V / \sqrt{n_{\text{pulse}}} \tag{9}$$

for  $n_{\rm pulse} = R\tau$ ,  $\eta_{\rm D} = 1$ , and  $K_{\rm conf} = 3$ . A useful figure of merit for the voltage sensitivity of photoemission and electron-beam sampling is [18]

$$G = \Delta V \sqrt{n_{\text{pulse}}} \,. \tag{10}$$

The number of pulses over which a signal must be summed to achieve a desired voltage resolution  $\Delta V$  then is

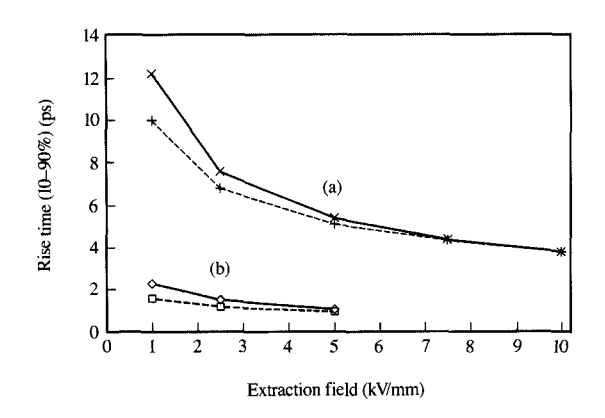
$$n_{\text{pulse}} = R\tau = (G/\Delta V)^2. \tag{11}$$

Thus, for a spot of 0.5- $\mu$ m diameter and a 1-ps pulse we have G = 0.6 V as the theoretical limit. Experimentally, a value of G = 2 V has thus far been demonstrated. The difference is related to the fact that noise sources other than shot noise contributed to the measurement and that the real detector efficiency  $\eta_D$  is of course smaller than 1.

Experimentally demonstrated values of G for electronbeam sampling with picosecond pulses are G = 66 V for an "effective" beam diameter of 0.5 µm and a kinetic energy of 2 keV for the primary electrons when a beamblanking system is used [4, 5], and G = 30 V for a raw beam diameter of 0.1 µm and a kinetic energy of 1.8 keV for the primary electrons when a laser-pulsed photocathode is used [26, 27]. The "effective" beam diameter in the first method accounts for beam instabilities which must always be considered in electronbeam probing, since even electric and magnetic fields generated on the chip under test itself may deflect the primary electron beam [28]—a problem which does not exist for photoemission probing. Therefore, electronbeam experts usually require a safety factor of 4 to 5 in spot size [2, 4], and the two results mentioned should thus belong approximately to comparable experiments. Theoretical values of G for electron-beam sampling with a laser-pulsed photocathode are about G = 15 V for a spot size of 0.1 µm and a kinetic energy of 1 keV for the incident primary electrons. G is inversely proportional to the square root of the energy of the incident primary electrons. The generally much smaller value of G for photoemission probing as compared to electron-beam probing is mainly related to the much smaller shape factor S in photoemission probing. Hence, better voltage sensitivity is an inherent advantage of photoemission probing. Since the safety factor of 4-5 is not needed for photoemission probing (see the subsection on minimum accessible feature size), photoemission sampling outperforms electron-beam sampling, even when the most effective version of the latter is used, by a factor of 15 (present experimental status) to 25 (theoretical limits) in G. Hence, electron-beam sampling needs 225 to 625 times more pulses to achieve the same voltage resolution  $\Delta V$ . This advantage of two to three orders of magnitude in the number of required pulses, or in signal integration time for a fixed pulse-repetition rate, is the main advantage of photoemission probing.

# • Time resolution

With respect to time resolution, one must distinguish between measurements in the real-time mode and measurements in the stroboscopic sampling mode. In the real-time mode, the incident beam of primary particles is continuous, and the time resolution is given by the reaction time of the voltage detector and the voltage sensitivity of the method. In any case, the signal frequency must be less than a few MHz. For fast signals, the stroboscopic sampling mode must be applied. As already mentioned, this mode can be applied to periodic signals only. The fastest measurable signal in this mode is determined by three factors: the length of the probing pulse, the so-called transit-time effect, and the time jitter





Dependence of the transit-time effect on the extraction field applied to the emitted electrons. Two different arrangements of conducting lines are considered for two different electron-start energies: (a) the three-line structure of 1- $\mu$ m width and spacing for 0-eV (solid line) and 8-eV (dashed line) start energy; (b) two coplanar lines of 1- $\mu$ m width and 2- $\mu$ m spacing for 0-eV (solid line) and 8-eV (dashed line) start energy. The input signal is idealized as a step-function. Adapted from [17].

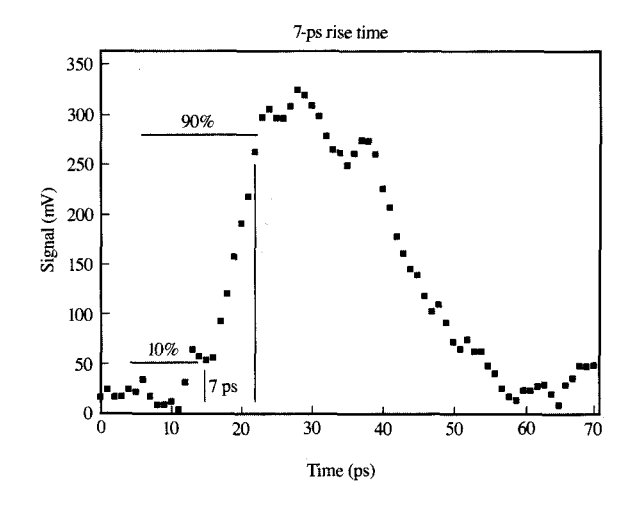


## Figure 2

Photoemission sampling measurement of a picosecond pulse on a coplanar strip-line of 5- $\mu$ m width and spacing. The pulse was generated by inducing a photoconductive short between the two biased coplanar lines with the 2.5-eV visible laser beam. The extraction field was approximately 1 kV/mm. From [17].

between the signals and the probe pulses. For an accurate measurement of the time in which a signal rises from 10% to 90% of its amplitude, the length of the probe pulse must not exceed 0.2 times the rise time of the signal [29]. Accepting an error of about 9% in the 10–90% rise time still requires that the length of the probe pulse does not exceed half the rise time of the signal [29]. Therefore, measurements of signals rising in less than 10 ps require probe pulses between 2 and 5 ps, depending on the desired accuracy. A time resolution of 5 ps requires probe pulses of about 2 ps or shorter duration.

The second limit to the time resolution, the transittime effect, shows a more complicated behavior. It depends strongly on the geometry of the metal lines on which the signal is measured, the extraction field applied to the emitted electrons, and the genuine rise time of the signal. The origin of the effect is that the kinetic energy of the emitted electrons upon reaching the reference or retarding electrode is given by the path integral over the electric fields along the electron trajectory, which deviates from the potential difference between start and end point of the electron trajectory if the potentials changed during the movement of the emitted electron toward the reference electrode. Practically, the kinetic energy gained by the electrons measures the potential at the point of electron emission in a weighted average over the time when the electrons are still close to the sample. A detailed analysis of the effect was published in 1987 [20, 21]. Figure 1 shows the smallest resolvable rise time (10-90%) as a function of the extraction field applied to the electrons for a metal line of 1-µm width surrounded by two equal lines in 1-µm spacing and for a coplanar transmission line. The curves are shown for electron start energies of 0 and 8 eV. For photoemission sampling, electron start energies lie between 0 and 1 eV, while in electron-beam sampling the corresponding peak in the energy distribution of the electrons may be at 8 eV or slightly higher. Figure 1 shows that both methods require extraction fields of a few kV/mm to measure signals rising in less than 10 ps on general chip structures. Only special line structures such as coplanar transmission lines of submicron width and spacing allow the measurement of signals shorter than 1 ps. The reason is the dipole-like field of a coplanar transmission line where one line carries the signal and the neighbor line the negative signal. This field decays very strongly with increasing distance from the lines, and therefore results in a very small transit-time effect. Figure 2 shows a signal generated by a photoconductive short between two coplanar transmission lines of 5-µm width and spacing. The 10–90% rise time is about 7 ps. The autocorrelation of the laser pulses which generated and probed this signal was about 2 ps; the remaining time is related to the transit-time effect for emission from 5-µm-wide coplanar

**Table 1** Feature size and voltage error in photoemission probing. The probe laser ( $\lambda = 248$  nm) is assumed to be focused exactly on the middle line of a symmetric structure of three coplanar metal lines of indicated width and spacing. The intensity distribution is given by the Airy distribution [Equation (14),  $\epsilon = 0$ ] for N.A. = 0.45.

| Width w <sub>1</sub> (µm) | Spacing w <sub>2</sub> (µm) | Error<br>signal |
|---------------------------|-----------------------------|-----------------|
| 0.36                      | 0.4                         | 0.1             |
| 0.36                      | 0.65                        | 0.06            |
| 0.5                       | 0.5                         | 0.03            |
| 0.5                       | 1.0                         | 0.01            |
| 1.0                       | 0.5                         | 0.01            |
| 1.0                       | 1.0                         | 0.008           |

transmission lines. The time jitter between probe pulse and signal is negligible, since the signal was generated by the same 2.5-eV laser pulse which also produced the 5-eV probing pulse by second-harmonic generation.

Of course, in general the time jitter is not negligible, but must be taken into account. This is an engineering issue which still needs to be analyzed and improved for general applications. We do not treat this aspect here.

# • Minimum accessible feature size

To estimate the minimum size of the features to which photoemission probing can be applied, we must consider some aspects of the method. In photoemission probing, experimental errors due to the finite probe size occur only if photoelectrons are emitted from a region surrounding the test point but on a different potential. On integrated circuits, the area between signal lines is primarily covered by insulators with work functions above 5 eV. Since photons with energies in the range 4.6  $eV < h\nu < 5$  eV are commonly used for photoemission probing, these insulators do not contribute to the photoemission current at all and cannot disturb the voltage measurement. Therefore, the main source of errors due to the finite probe size of the laser beam is photoelectrons emitted from metal structures in the vicinity of the structures under test. Since other perturbation effects are unavoidable (see the following subsection), contributions from these lines can be accepted as long as the effect is small compared to these other effects. Such voltage errors caused by overlapping laser beams can be described [30] by

$$|\Delta V_{s}| = \left| \sum_{i} (V_{s} - V_{i}) \frac{I_{i}}{I_{s}} \right| \le \left( \sum_{i} \frac{I_{i}}{I_{s}} \right) \Delta E/e$$

$$\le \frac{\left[ 1 - E_{\text{edge}}(\frac{1}{2}w_{1} + w_{2}) \right]}{E_{\text{edge}}(\frac{1}{2}w_{1}) - \frac{1}{2}} \Delta E/e, \tag{12}$$

where  $\Delta V_s$  is the inaccuracy of the signal  $V_s$  to be measured,  $I_i/I_s$  is the ratio of the laser intensity on the *i*th

neighbor line to the intensity on the signal line under test,  $V_i$  denotes the voltage at the *i*th line,  $w_1$  is the width of the line under test,  $w_2$  is the spacing to the closest neighbor line, and  $\Delta E$  is the width of the energy distribution of the photoemitted electrons.  $E_{\rm edge}$  is the edge-resolution function which gives the total intensity of the incident laser beam passing the edge of a semi-infinite plane extending from x to  $+\infty$ ,

$$E_{\text{edge}}(x) = \frac{1}{E_{\text{edge}}(\infty)} \int_{-\infty}^{x} \int_{-\infty}^{\infty} I(r = \sqrt{x'^{2} + y'^{2}}) dy' dx'. \quad (13)$$

Equation (12) gives an upper limit for the voltage error and is based on the assumption that the photoemission signal is linear in  $V_s$  and  $V_i$ . This implies an appropriate setting of the retarding voltage of the electron detector for selecting an operation point in the linear part of the detector characteristic (S-curve).

For calculating actual voltage errors based on Equation (12), we consider a lens with an annular aperture homogeneously illuminated with light. Here, the radial distribution I(r) of the intensity in the focal plane can be described in the ideal case of diffraction-limited (aberration-free) imaging [31] by

$$\frac{I(r)}{I_0} = \frac{1}{(1 - \varepsilon^2)^2} \left[ \frac{2J_1(kr)}{kr} - \varepsilon^2 2 \frac{J_1(\epsilon kr)}{kr} \right]^2, \tag{14}$$

where  $I_0$  is the maximum intensity at r=0,  $J_1$  is the first-order Bessel function, k is defined as  $k=2\pi/\lambda$  N.A. ( $\lambda$  is the wavelength of light and N.A. indicates numerical aperture), and  $\varepsilon$  denotes the "obscuration ratio"  $r_1/r_2$  of the annular aperture, where  $r_1$  and  $r_2$  are the radius of the central obscuration and the outer radius of the free aperture, respectively.

Equation (14) has been extensively discussed in the literature for the special case  $\varepsilon = 0$ , which is equivalent to imaging through a circular aperture (with no central obscuration). For  $\varepsilon = 0$  the intensity distribution (14) is simply proportional to  $[J_1(kr)/(kr)]^2$  (the so-called Airy distribution), which is a damped oscillatory function of r with a series of zeros.

The maximum voltage error according to the right side of Equation (12) is listed in **Table 1** for different widths  $w_1$  of the line under test and different spacings  $w_2$  to the closest neighboring lines assuming diffraction-limited N.A. = 0.45 optics,  $\lambda$  = 248 nm, and a diffraction pattern given by the Airy distribution [Equation (14)]. All values for  $w_1$  and  $w_2$  have been chosen in the range below 1  $\mu$ m. Obviously, diffraction-limited N.A. = 0.45 optics should allow photoemission probing measurements on 0.5- $\mu$ m lines with 0.5- $\mu$ m spacings, with errors less than 3% of the differences between the signal to be measured and the voltage on neighboring lines. This is an acceptable value,

comparable to errors which must be attributed to purely electrostatic crosstalk effects on microstructures which are unavoidable even if "advanced" electron detector schemes are used.

An obscuration of the aperture leads to a broadening of the intensity distribution in the focal plane. This effect is shown in **Figure 3** for the special case of homogeneously illuminated annular apertures. The figure shows the equivalent edge-resolution curves  $E_{\rm edge}$ . Thus, to achieve the best resolution on extremely dense structures, lens systems without obscuration of the aperture are definitely favorable.

Figure 4 shows a corresponding edge-resolution measurement with our photoemission probing system based on a mirror objective with N.A. = 0.45 and a central obscuration ratio of 0.5. The signal changes from 90% to 10% of its maximum amplitude in  $0.85 \pm 0.05$   $\mu$ m. This is very close to the theoretical value of 0.8  $\mu$ m for this objective and demonstrates that the theoretical limits can be achieved in practical systems.

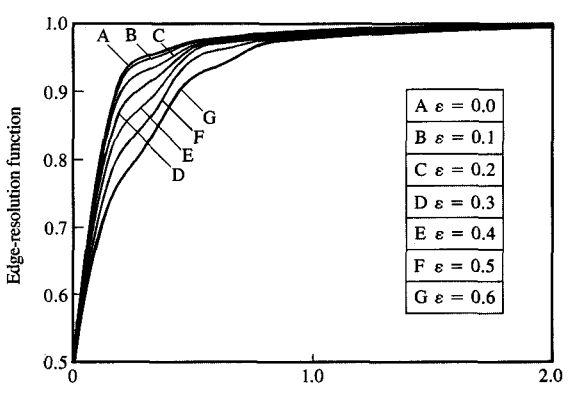
Obviously, the limits of "spatial resolution" indicated in Table 1 can be slightly improved by using higher N.A. optics (N.A. > 0.45) and a shorter wavelength. In any case, these limits allow access to metal lines of a few tens of micrometers in width and spacing with errors small in comparison to other unavoidable errors. At this point we should mention that these values require a very good control for keeping the sample in the focal plane of the lens, since misalignments of the order of a micron already result in a doubling of the beam diameter on the surface of the device under test.

# • Sensitivity to perturbation effects

There are three general effects which perturb signal measurements on integrated circuits by photoemission or electron-beam probing: the crosstalk effect, the local barrier effect, and the influence of surface contaminations.

# Crosstalk effect

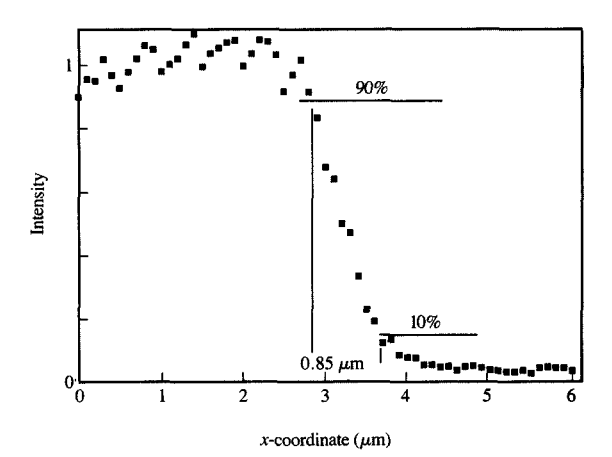
The crosstalk effect can be divided into the static [32] and the dynamic [20, 21] crosstalk effects. The static crosstalk effect results from dependencies of the trajectories of the emitted electrons on the voltages applied to conductors close to the point under test. This influence results in changes of the angle with which the electrons reach the retarding field detector, and may therefore result in changes in the voltage measurement. The effect is quite strong for planar retarding field detectors, but can be reduced to small values by special detector designs. For photoemission probing we have developed such a special detector, which is extremely insensitive to static crosstalk effects [30]. Figure 5 shows a crosstalk measurement on a comb structure containing



Distance x from center  $(\mu m)$ 

#### Figure 3

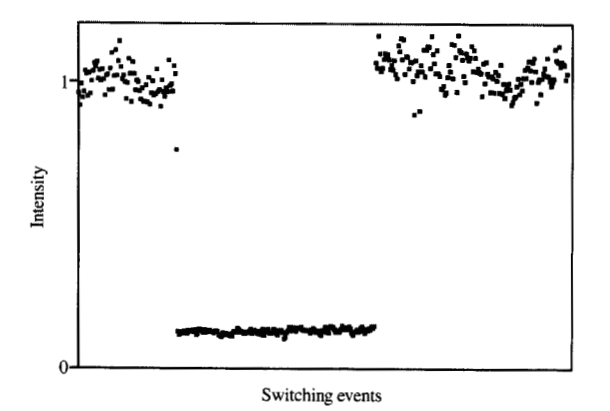
Edge-resolution curves  $E_{\rm edge}(x)$  calculated with Equation (13) for the intensity distribution in the focal plane of homogeneously illuminated objectives with annular apertures of different obscuration ratios  $\varepsilon$  as given by Equation (14). Parameters: N.A. = 0.45,  $\lambda$  = 248 nm. Adapted from [30].



#### afailte 1/2

Photoemission intensity in a one-dimensional scan from a metal line to a  $SiO_2$  insulator. The intensity drops from 90% to 10% within  $0.85\pm0.05~\mu m$ . From [17].

metal lines of  $1-\mu m$  width and spacing. The comb is divided into two subcombs, so that the two neighboring lines of any line selected always belong to the other comb

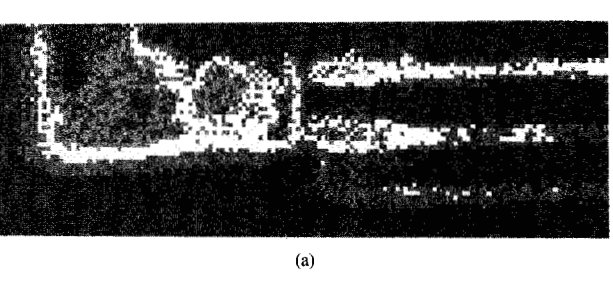


## STOTE V.

Static crosstalk measurement on two entangled combs of  $1-\mu m$  width and spacing. The photoemission intensity is measured for emission from one line. All lines are on 0 V at the beginning; then the voltage at the emitting line and all other lines of the connected comb is changed from 0 to 2 V (first large signal change); then the voltage on the intertwined comb structure is changed from 0 to 2 V (in the middle of the low-intensity region); then the voltage on the comb structure with the emitting line is changed back to 0 V (second large signal change); and finally, the voltage on the second comb is changed back to 0 V (in the middle of the remaining part). Adapted from [19].

than the line under test. The two subcombs may be connected to different potentials. Figure 5 shows the change in photoemission intensity for a fixed retarding voltage when, first, the potential of the line under test is changed, and second, the potential of the neighboring lines is changed by the same potential difference. Both the minimum and the maximum intensity value are chosen clearly in the linear range of the detector characteristics (S-curve). It is obvious that the static crosstalk effect on the photoemission signal is less than 5% of the real signal. More accurately, we can give only this upper limit, since the crosstalk effect disappears in the statistical noise of the measurement. In the shot-noise limit, the noise at the high-intensity value should be about three times the one at the low-intensity value. The observed somewhat larger noise at high intensity is probably due to additional noise from the channeltron electron detector, which is not well suited for such a high number of electrons. One should point out that these measurements on comb structures, where every second metal line is changing voltage at the same time, correspond to half of the worst case, i.e., the case of a bus structure where all neighboring lines change voltage at the same time. The effect was similar whether the signal was measured on a line in the middle of the comb

structure or at the edge. It also was similar when the experiment was performed on a comb structure with lines of 4- $\mu$ m width and spacing instead of 1  $\mu$ m, thereby indicating that the effect scales with the ratio between line width and line spacing. Accordingly, a larger crosstalk effect is measured near larger conducting structures, as can be seen in Figure 6(a). This figure shows a false-color plot of the difference between two two-dimensional voltage-contrast scans on the comb structure of 1-μm width and spacing, one with both combs at 0 V, the other with one comb at 0 V and the second at 2 V. The scan is made in a region where an approximately 4-µm-wide metal line connects one comb to the input pad where the signal is changed from 0 V to 2 V. The geometry is shown in Figure 6(b). The comb which is connected to the metal line consists of polysilicon, and no photoemission occurs from these lines since the work function of the material is larger than the used photon energy of 5 eV. A large crosstalk signal is visible close to the wide metal line which decreases strongly with increasing distance from the line. Also, the metal line more to the lower edge of the figure shows a crosstalk signal that is clearly smaller than those of the two lines at the same height as the wider line.



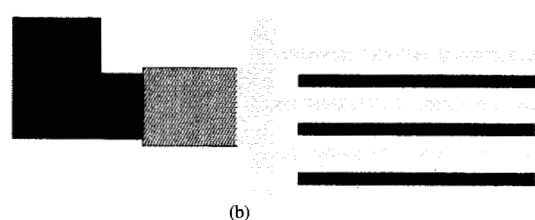


# Figure 6

(a) False-color plot of the difference between two two-dimensional voltage contrast scans for different voltage arrangements on two entangled conducting comb structures. Red corresponds to zero potential difference between the two scans; red changing to yellow corresponds to small changes. The potential difference increases from yellow to green and finally to blue and dark-blue, which correspond to the full 2-V change of the potential. Each deviation from zero in the right-hand side of the picture is caused by static crosstalk. (b) Geometry of the entangled comb structure. Blue regions represent metal structures, the yellow region the polysilicon areas, and the green region in the center the connection from the polysilicon comb to the wide metal line.

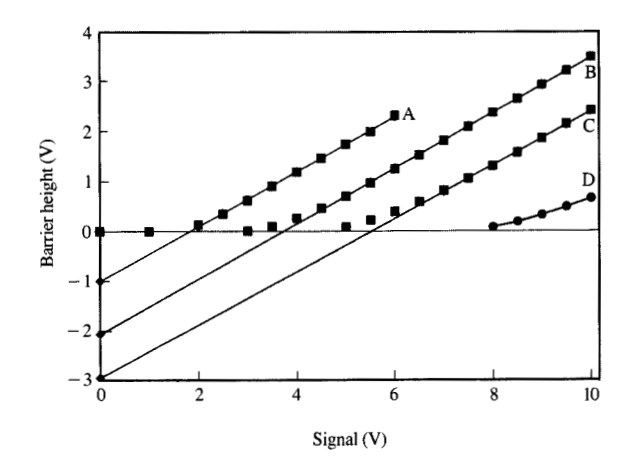
The dynamic crosstalk effect, like the transit-time effect, stems from the nonconservation of energy in time-dependent fields, but is caused by the changes in the potential at neighboring lines rather than at the line under test itself. It shows a dependence on geometry, genuine input signal, and extraction field similar to that of the transit-time effect and is of comparable magnitude for photoemission and electron-beam sampling [21]. Like the capacitive coupling from signals on one line to those on a neighboring line, the effect occurs only with changing signals on a neighboring line; thus, it may be hard to distinguish these effects in practice.

# Local barrier effect

For small extraction fields, it can happen that the static crosstalk effect cannot be avoided by special detector concepts, and that it even leads to a total suppression of the photoemission signal if the signal voltage at the line under test is much more positive than the voltage at the neighboring lines. This is caused by a local potential barrier building up in front of the line under test as a result of the extension of the higher-potential-energy regions from the neighboring lines into the region in front of the line under test [32]. At the line under test itself, the electrons are at a lower potential energy than at the neighboring lines. If the induced potential energy in front of the line exceeds that of the line itself somewhere along the trajectories of the emitted electrons, electrons of lower kinetic energy cannot leave the device. If there is a point where the potential barrier exceeds the maximum start energy of the electrons, the photoemission signal from this line is totally suppressed. The size of the induced local potential barrier depends on the geometry of the lines, the extraction field applied to the electrons, and the voltage applied to the neighboring line. The effect is strongest for a geometry with many lines of small spacing, since larger areas of open dielectric material assume high negative values of potential energy relative to the potential of the extraction electrode close by. The high negative potential energy values eliminate local barriers. Figure 7 shows the induced local potential barrier as a function of the voltage applied to the signal line when the voltages on all neighboring lines are kept fixed at zero. The barrier height is shown for different extraction fields. The geometry is that of a many-line structure of 1-µm width and spacing, and the barrier is considered at a central line. It is clear that minimum extraction fields between 1 and 5 kV/mm are required to reduce the local barrier to zero if the voltage at the signal line exceeds that of the neighboring lines by 1 to 8 V.

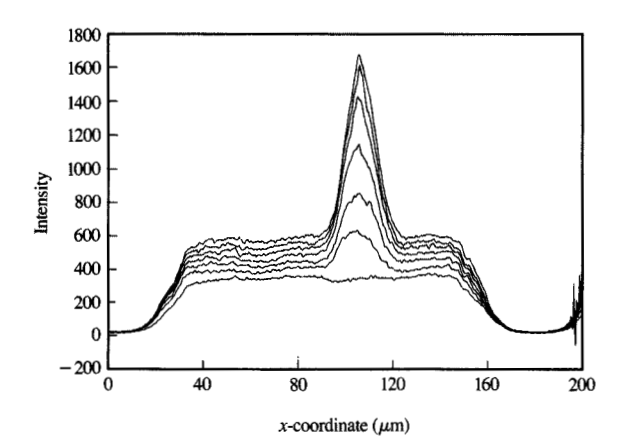
## Influence of surface contamination

Photoemission is known to be a very surface-sensitive method and has made large contributions to the



Local barrier height induced in front of a signal line surrounded by many lines on zero potential as a function of the voltage applied to the signal line for extraction fields of 1 (curve A), 2 (curve B), 3 (curve C), and 5 kV/mm (curve D). Each line is  $1\mu m$  wide; the spacing to the neighbor line is also  $1\mu m$ . The lines are  $1\mu m$  high and are insulated by a  $0.5\text{-}\mu m$  SiO $_2$  layer from a thick Si substrate with ground plate. The barrier in front of the signal line is generated by the lines held at zero potential.

understanding of surface states and surface band structures as well as other surface-related effects. However, in photoemission probing this sensitivity can cause severe problems with respect to the stability and reliability of the measurements. It is therefore imporant to clarify the dependence of photoemission probing measurements on the surface conditions of the sample. A series of investigations have been performed to establish these dependencies. Figure 8 shows the changes in photoemission intensity in scan measurements over an air-exposed gold pad. Here, one spot of the metal pad is illuminated with a high-intensity laser beam, and the pad, including this spot, is scanned after different illumination times for the spot selected. While the intensity on the metal is very homogeneous in the scan before illumination, an intensity peak evolves during laser illumination at the spot on which the beam was focused, and also the intensity from the rest of the pad increases after each laser scan across the pad. It is obvious that laser illumination changes the contamination on the metal surface. To verify this effect, we measured the photoelectron energy distribution directly by modulating the retarding voltage of our retarding field detector. The spectra were taken with laser intensities reduced by a factor of 10 to avoid contamination changes during



# Flaure 8

Photoemission current in scans over a metal pad surrounded by insulator as a function of laser illumination. The laser beam was focused for 5 min on a spot at about the  $110-\mu m$  mark between successive scans.

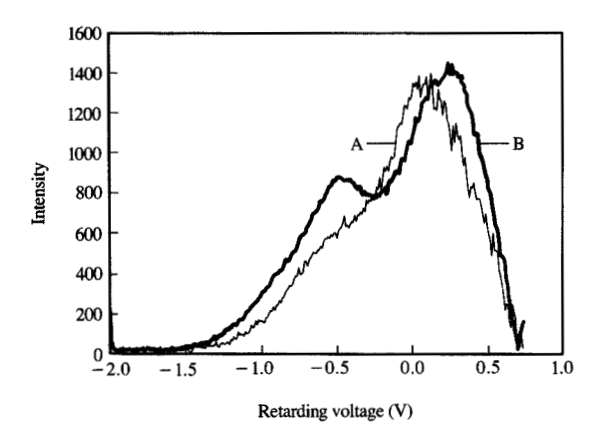


# Figure 9

Photoemission spectra measured by modulating the retarding field voltage before (curve A) and after (curve B) strong laser illumination of a metal pad on an air-exposed sample.

measurement. Some spectra for emission from the Au are shown in Figure 9. There is a main peak at low kinetic energy (= high retarding voltage) and a small shoulder at higher kinetic energies (= lower retarding voltages) for short illumination times. This shoulder evolves into a peak with increasing illumination time. The small shifts

of the main peak to lower kinetic energies may reveal a small decrease of the work function with increasing laser illumination time. The increase of the high-kinetic-energy peak should be related to an increase of occupied electron states close to the Fermi energy. Therefore, we tend to the conclusion that the contamination of the surface is reduced or changed with illumination time, thereby returning electrons which heretofore were bound at higher chemisorption orbitals (out of the energy range accessible with our photon energy) to states close to the Fermi energy. Since clean Au should have a much larger work function, it is clear that there still is contamination, but probably less than before. The time dependence of the photoemission signal when a single spot on the gold pad is illuminated is shown in Figure 10. Here, a highintensity laser beam is focused on the air-exposed gold pad. A steady increase of the current up to a saturation level is observed for the dirty sample, while after ionetching a nearly constant current is observed. The etching was performed in a vacuum of only  $5 \times 10^{-7}$  mbar, and at least 10 minutes passed between the etching and the subsequent photoemission measurement.

The results indicate that the surface sensitivity of the method must be taken into account for air-exposed samples if the measurement time on a single spot of the sample exceeds a few seconds. The effect is also important in scanning over the sample, since even the low-intensity wings of the laser-beam distribution already affect the surface contamination. However, the effect can be suppressed by ion-etching of the samples even under practical vacuum conditions. A similar effect is observed in electron-beam probing of air-exposed samples. The differences seem to be that there the signal decreases with irradiation time, and that even initially clean samples are contaminated by hydrocarbons produced by the cracking of residual gas components by the incident electron beam [33]. Here the situation is more severe for electron-beam probing than for photoemission probing.

#### • Impact on the circuits under test

# Impact of ultraviolet light

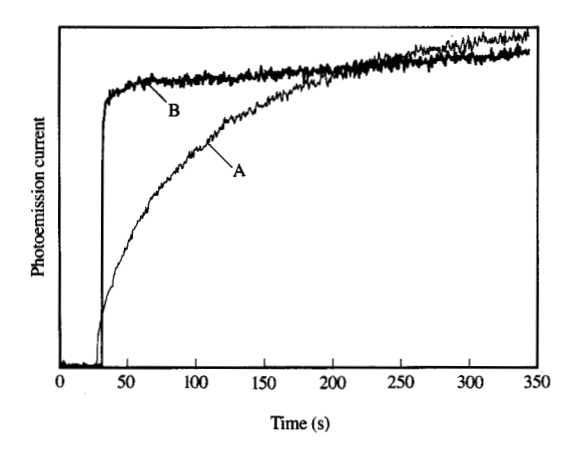
As the impact of electron-beam irradiation on devices is known in electron-beam probing [34], the principal impact of light on devices is also well known and causes permanent as well as momentary changes. Momentary changes are caused by the electron-hole pair generation, which through separation of electrons and holes in the local fields inside a device causes electrical currents which may perturb device operations as soon as certain current limits are exceeded. Related to this effect are, e.g., changes of the breakdown voltage of transistors and diodes. Permanent changes are caused mainly in MOS structures, where the generated electrons or holes may

penetrate into the oxide and change the overall potentials in the device by filling trap states in the oxide which are always present. The important question concerns the magnitude of these effects as a function of the laser power used to excite photoemission, and also the limits in induced currents and voltage shifts which can be accepted without affecting device operation. The impact of ultraviolet (UV) light should be much smaller than that of visible light, because of the usually higher absorption of the UV light in insulating and semiconducting layers above the active device regions. This is especially true when the insulating material is polyimide. Here the transmission probability drops to very small values for wavelengths below 350 nm. The absorption coefficient is about  $2.3 \times 10^5$  cm<sup>-1</sup> for a wavelength of 250 nm corresponding to a photon energy of 5 eV. Experimental studies of the effects revealed no impact on CMOS chips with polyimide insulating layers.

In experiments on bipolar technology with UV-transparent oxide and nitrite layers as insulators, UV light induced electron-hole pairs, which produced junction leakage currents and junction breakdown voltage reductions in reverse-biased junctions, as well as photovoltage generation in nonbiased junctions. The effects observed until now seem to be small compared to the operating currents in the devices analyzed. More extensive studies on the impact of UV radiation on various device technologies with UV-transparent insulators are required for a final conclusion, while the applicability to devices using polyimide or similar insulators seems to be clear. Of importance here is that very fast devices primarily use polyimide because of the much lower dielectric constant of this organic insulator.

# Impact of high extraction fields

The requirement to apply a high extraction field in picosecond time-resolution measurements for electronbeam or photoemission sampling raises questions about compatibility with integrated circuits. An investigation of the influence of high electrostatic fields was performed on CMOS and GaAs-MESFET devices. To simplify the experimental setup, the measurements were done in air. The electrode was a polished metal cylinder of 0.5-mm diameter, which was placed 15  $\mu$ m above the devices under test. The electrical performance of the devices was monitored with a standard IV-curve tracer. The applied fields were 0 and 25 kV/mm. This is at least a factor of 4 higher than what is required in picosecond sampling. According to Figure 1, there is no significant reduction in transit-time effect for fields higher than 5 kV/mm. The results of the IV measurements of the two types of devices were identical for applied fields of 0 and 25 kV/mm. This insensitivity can be explained by the shielding of sensitive channel regions by the closely



Time dependence of the photoemission current from an air-exposed sample before (curve A) and after (curve B) ion-etching of the sample. The laser beam was turned on at about the 30-s mark.

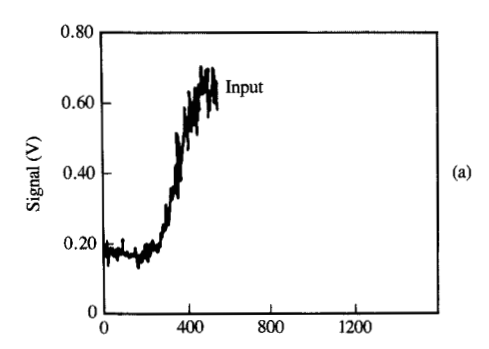
spaced metal lines. A calculation of the field strength vertically to coplanar metal lines indicated a sharp decay very close to and between the lines. The area below the lines was almost free of field.

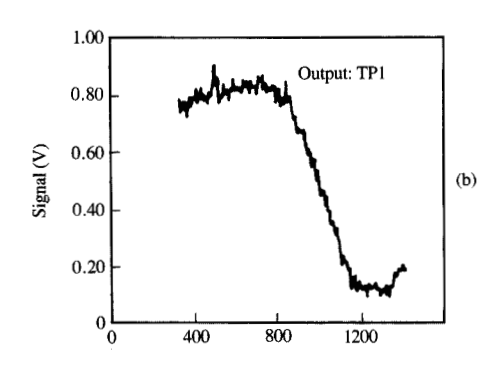
In conclusion, no device impairment is expected when a static extraction field is applied, because of the screening of such fields by the closely spaced conducting lines on integrated circuit chips. This screening is especially effective in chips with several metallization layers between the field-sensitive devices and the chip surface.

#### Device loading

In contrast to the electron-beam method, photoemission probing extracts electrons from the device under test without having the possibility of balancing the extracted electron current by the incident primary beam. It is therefore important to estimate the corresponding influence on device operation as well as the voltage measurement itself. Considering the optimum arrangement for a spot size of 0.5- $\mu$ m diameter, about 55 electrons are extracted from the device with each picosecond pulse.

Two cases must be distinguished. In the first, when a signal waveform is measured, the signal is reproduced with its repetition rate, which equals the repetition rate of the incident laser pulses. Hence, each produced signal is influenced by one single pulse only. If the device has an output capacity of 100 fF, the photoemitted electrons reduce the voltage of each signal by  $88 \mu V$ —an effect





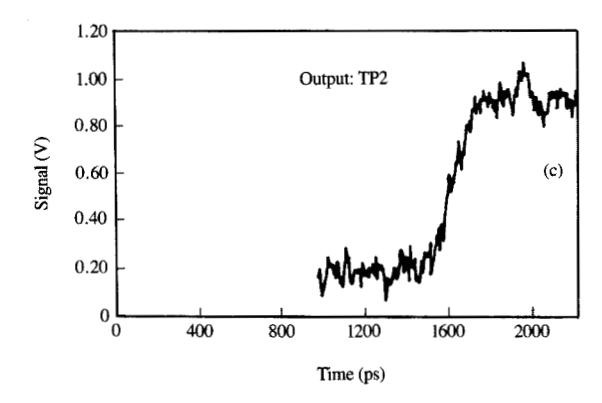


#### Figure 11

Signal measurements on an inverter chain of a GaAs MESFET: (a) the electric input pulse to the inverter chain generated by a photodiode with the pulses of the visible 2.5-eV laser beam; (b) the signal measured at the output of the first inverter in the chain; (c) the corresponding signal measured at the output of the fourth inverter. From [19].

which should be negligible for the device and also for the accuracy of the voltage measurement. If the output capacity of the device is lower, e.g., 10 fF, the effect

increases to, e.g., 880  $\mu$ V. But even this value should be negligible.

In the second class of measurements, the signal is not repeated but kept constant. Such measurements could be used for determining the leakage rate of a storage cell. Here, each laser pulse would successively change the voltage at the storage cell. Even with the theoretical limit of G = 0.6 V, 400 pulses would be needed to resolve 30 mV. At the same time, the photoemission process would change the voltage of the storage cell by 35 mV if the capacity were 100 fF. However, the effect of the photoemission process is known if the capacity of the storage cell is known and thus can be included in the interpretation of the measurements. Problems occur only if the capacity of the device or the photoemission intensity is not known with sufficient accuracy, or in test applications where changed information in a memory cell unpredictably influences the operation of the circuit under test.

# 4. Range of applications

The possible applications for contactless probing on internal nodes of integrated circuits range from waveform measurements on single nodes to voltage-contrast measurements in various modes [1-3]. As an example, Figure 11 shows rise-time and delay measurements on internal nodes of a GaAs MESFET chip by photoemission sampling [19]. The device under test is a chain of inverters which are triggered by an input signal produced by a 2.5-eV laser beam on a photodiode, while the pulses of the 5-eV laser beam used for the photoemission probing measurements are produced from those of the 2.5-eV laser beam by frequency doubling. This special way of synchronizing the probe pulses with the signal under test practically eliminates the time jitter. A special kind of application may evolve from the possibility of using the 2.5-eV laser beam to switch a discrete device on a circuit, as for example in the opticalbeam-induced-current (OBIC) method [35, 36], and to measure the reaction of this discrete device directly by photoemission sampling at the output of the device. Such a measurement is shown in Figure 12. Here, the output signal of one inverter was measured after a transistor in this inverter was triggered by the 2.5-eV laser beam and then again after a transistor of the preceding inverter in the chain was triggered by the same beam. In the following, we focus on the conventional applications of photoemission probing in comparison to electron-beam probing rather than on the combination with OBIC.

The key parameters which determine the range of applications for a specific contactless probing method are voltage sensitivity, time resolution, minimum accessible feature size, sensitivity to perturbation effects, and impact on the circuit under test, i.e., all the issues discussed in

Section 3 for photoemission probing. There we have seen that the time resolution is about the same for photoemission and electron-beam probing, and also that metal lines down to 0.5-µm width and spacing or slightly smaller can be tackled by both methods. The sensitivity to perturbation effects such as crosstalk and surface contamination is also similar. The impact of ultraviolet light as well as electron beams on circuits is known, but seems to be acceptable in both methods. In particular, the very fast devices using insulating layers of polyimide showed no reaction to 5-eV laser beams in photoemission probing experiments. Hence, there are two general effects which distinguish the range of applicability of photoemission probing from that of electron-beam probing. The first effect is the possible deflection of the primary electron beam by electromagnetic fields generated on the chip under test itself, which leads to significant problems in dynamic VLSI probing by electron beams [37]. Here is an inherent advantage for photoemission probing which may even lead to a better spatial resolution for dynamic photoemission probing than for dynamic electron-beam probing of VLSI chips. The second effect is the very high voltage sensitivity of photoemission probing. In the following we concentrate on the issue of voltage sensitivity and its significance for different applications. To demonstrate this significance, let us compare the resulting measurement times of photoemission sampling and electron-beam sampling with conventional beam blanking [4, 5] and with a laserpulsed photocathode [26, 27].

For the advanced electron-beam probe in [4], an effective electron-beam diameter of 0.5 µm is introduced, corresponding to a raw beam diameter of 0.1 µm plus the inclusion of the safety factor of 4 to 5 (see the subsection on voltage sensitivity). This is comparable to the  $0.1-\mu m$ raw beam diameter of electron-beam probing with a photocathode [26, 27]. By keeping the probe beam diameter constant for  $0.5-\mu m$  feature size, the remaining parameters can then be balanced against one another for high time resolution, high voltage resolution, or short measurement time. The pulse duration in photoemission sampling has been measured by autocorrelation to be within 1 to 2 ps full width half maximum (FWHM), while for the photoemission cathode a few more picoseconds must be assumed (see [23]). The signal-tonoise ratio of conventional electron-beam sampling used in this comparison was measured with a pulse duration of 7 ps [4], but was subsequently improved to about 3-4 ps [5]. For the sake of convenience, the time resolution is therefore assumed to be roughly the same in all three cases. The performance of the photocathode method used here has been achieved by modulating the rate of the device clock while keeping the laser clock constant. The result is an improvement by a factor of 6.6 for voltage

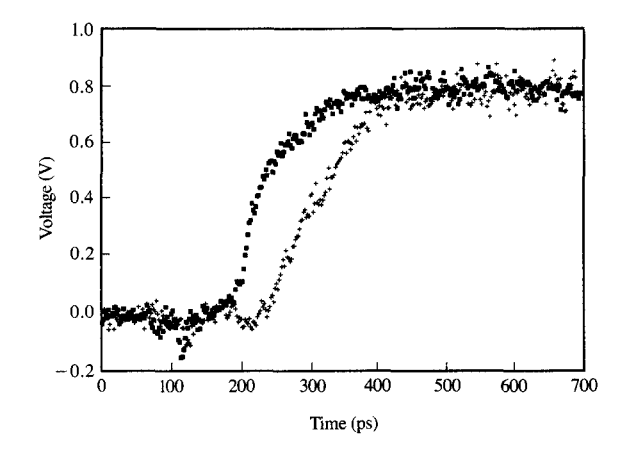
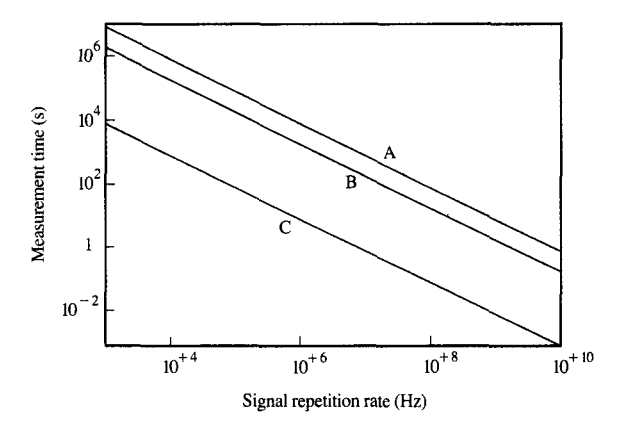


## Figure 12

Signal measurements on an inverter chain of a GaAs MESFET. The inverters are triggered optically with the pulses of the visible 2.5-eV laser beam focused onto one of the transistors of the same inverter where the output signal is measured (squares) and of the preceding inverter in the chain (crosses). Adapted from [19].



Measurement time as a function of the sampling pulse rate, i.e., the signal-repetition rate for measuring a voltage slope consisting of 200 points with 10-mV resolution on a single node. Curve A= electronbeam sampling with beam blanking; curve B= electronbeam sampling with a laser-pulsed photocathode; curve C= experimentally demonstrated values of photoemission sampling for a beam diameter of 0.5- $\mu$ m FWHM.

sensitivity, or 44.5 in measurement time. The method has been applied neither in photoemission probing nor in electron-beam probing with beam blanking. Figure 13

compares measurement times required by the three methods for voltage slopes consisting of 200 phase points with 10-mV resolution. The values have been taken from the published data for demonstrated figures of merit for voltage sensitivity, which are G=2 V for photoemission sampling with pulses of 1–2-ps duration [18, 28], G=30 V for electron-beam sampling with a laser-pulsed photocathode and a primary beam energy of 1.8 keV [26, 27], and G=66 V for electron-beam sampling with beam blanking and a primary beam energy of 2 keV [4, 5]. Design verification and failure analysis experts specify testing requirements down to 1-mV voltage resolution. For this case, the times given must merely be multiplied by a factor of 100.

From Figure 13 and [2-5], one concludes that signals with low repetition rates and large rise and fall times as well as signals with repetition rates close to 1 GHz and small rise and fall times can be covered by conventional electron-beam testers. The long rise time down to several hundred picoseconds allows longer sampling pulses with considerably more electrons, which in turn produce a signal-to-noise ratio sufficient to satisfy many applications. The same effect occurs for the fast signals with high repetition rates, where these repetition rates provide the large number of electrons needed to achieve the desired voltage resolution. Here, the use of the laserpulsed photocathode still improves the performance. The situation with fast signals and low repetition rates is where photoemission sampling comes in. Here, the benefit of the high voltage sensitivity of the photoemission tester can be fully utilized. The situation occurs in highly integrated circuits rather than in simple test structures to evaluate high-speed device performance. The projected data for the measurement time in Figure 13 show that if the repetition rate of a voltage slope under test drops to 100 kHz, it will take more than 27 hours to measure a voltage slope with 10-mV resolution, even for the laser-pulsed photocathode version of electron-beam probing. When a voltage resolution of 2 mV is required, this value even increases to 695 hours. Therefore, severe problems in measurement time must be expected for electron-beam sampling on full VLSI circuits, and photoemission probing is the candidate for these applications. VLSI chips, where special problems of this kind are expected, are complicated logic chips where repetition rates for the highest bits in logical operations can be below 1 MHz although the signals themselves are on the picosecond scale, or chips of hybrid analog-digital technology in telecommunication with the Integrated Services Digital Network (ISDN), where bit rates down to a few kHz or even lower must be dealt with. Examples of such complicated logic circuits are chips where levelsensitive scan design (LSSD) structures have been implemented to enable effective functional testing by

loading series of bit patterns into shift registers, and to analyze the output response of a complex logic onto these patterns. Here, if a certain pattern leads to a faulty response, the logic between the shift registers and the output channels is analyzed by internal node probing. To enable dynamic testing of the response, the corresponding pattern must be repeated periodically, with the pattern-repetition rate defining the repetition rate of the probe pulses in stroboscopic sampling measurements. Even if the clock rate is 100 MHz, a 100-bit pattern needs 1 us to be loaded into a shift register. Hence, the pattern repetition rate is only 1 MHz. Actual bit patterns consist of much more than 100 bits, and accordingly the repetition rates drop into the kilohertz range. Here, photoemission probing gives access to a range of applications which simply cannot be reached by electronbeam probing. Since this range of applications is based on chips with very fast devices, it can be expected that corresponding future chips will exploit primarily organic insulators, such as polyimide, because of their small dielectric constant, which is important for fast devices. Hence, this range of applications coincides with that in which photoemission probing has already proven its applicability. Even if future analyses of MOS circuits should reveal that there are some devices without organic insulators, which are sensitive to perturbations by ultraviolet light, this is not expected in the range of very fast devices in VLSI circuits, where the application of photoemission probing offers its special advantages over electron-beam probing.

# 5. Conclusion

In summary, the capabilities and limits of photoemission probing have been reviewed to locate the range of applications in which this novel contactless testing method offers signficant advantages over existing methods. It is concluded that this lies in the field of complex logic and telecommunication chips, where very fast signals may occur with low repetition rates which prohibit high-resolution analyses of these chips by electron-beam probing. The special advantage of photoemission probing in this field of applications originates from its inherently high voltage sensitivity. The minimum features accessible in photoemission probing are below 0.5  $\mu$ m for width and spacing of conducting metal lines. This allows application to the corresponding chips with no problems, since connection lines in the metallization layers will be larger in the foreseeable future. Also, sensitivity to perturbation effects and the impact of the circuit under test are considered to be at least as small as in electron-beam probing, although the impact of ultraviolet light on MOS devices without organic insulators needs further investigation. Another more general problem which must be considered with

respect to photoemission and electron-beam probing is the accessibility of arbitrary nodes on chips with many metallization layers. Possible solutions to this problem include the drilling of holes through insulating layers to reach lower-lying nodes, or special designs for testability which implement connections to special test pads on the chip surface.

# **Acknowledgments**

We thank R. Tibbetts and J. Wilczynski for designing the mirror lens used for submicron spatial resolution, and P. Müller for developing the software which controlled our experiments. We are grateful to W. Bucher, L. Perriard, H. Richard, and J. Rizzolli for technical support of this work, and to J. A. Kash, J.-M. Halbout, M. B. Ketchen, L. M. Geppert, J. D. Feder, and B. Van Zeghbroeck for providing us with samples for our experiments, as well as to all their colleagues involved in the design and fabrication of these samples.

#### References

- E. Menzel and E. Kubalek, "Fundamentals of Electron Beam Testing of Integrated Circuits," Scanning 5, 103-122 (1983).
- E. Wolfgang, "Electron Beam Testing," Microelectron. Eng. 4, 77-106 (1986).
- S. C. J. Garth, "Electron Beam Testing of Ultra Large Scale Integrated Circuits," Microelectron. Eng. 4, 121–138 (1986).
- M. Brunner, "Schnelle Elektronenstrahl-Messtechnik für Integrierte Mikrowellenschaltungen," Mikroelektron. 3/1988, 28-31 (1988).
- M. Brunner, R. Schmidt, and D. Winkler, "Characterization of ps-Electronic Devices: A Challenge for E-Beam Testing," presentation at the symposium on "Beam Testing of Circuits and Devices" at the Fall Meeting of the Electrochemical Society, October 9-14, 1988, Chicago, IL, unpublished.
- B. H. Kolner and D. M. Bloom, "Electro-Optic Sampling in GaAs Integrated Circuits," *IEEE J. Quantum Electron.* QE-22, 79-93 (1986).
- G. A. Mourou, "Picosecond Electro-Optic Sampling," High Speed Electronics, Springer Series in Electronics and Photonics, Vol. 22, B. Källbäck and H. Beneking, Eds., Springer-Verlag, Berlin, 1986, pp. 191–199.
- J. L. Freeman, D. M. Bloom, S. R. Jefferies, and B. A. Auld, "Sensitivity of Direct Electro-Optic Sampling to Adjacent Signal Lines," Appl. Phys. Lett. 54, 478-480 (1989).
- R. Clauberg, H. K. Seitz, A. Blacha, J. A. Kash, and H. Beha, "High-Speed Integrated Circuit Testing by Time-Resolved Photoemission," High Speed Electronics, Springer Series in Electronics and Photonics, Vol. 22, B. Källbäck and H. Beneking, Eds., Springer-Verlag, Berlin, 1986, pp. 200–203.
- H. K. Seitz, A. Blacha, R. Clauberg, and H. Beha, "Energy- and Time-Resolved Photoemission in a Promising New Approach for Contactless Integrated Circuit Testing," *Microelectron. Eng.* 5, 547–553 (1986).
- J. Bokor, A. M. Johnson, R. H. Storz, and W. M. Simpson, "High-Speed Circuit Measurements Using Photoemission Sampling," Appl. Phys. Lett. 49, 226–228 (1986).
- R. B. Marcus, A. M. Weiner, J. H. Abeles, and P. S. D. Lin, "High-Speed Electrical Sampling by fs Photoemission," *Appl. Phys. Lett.* 49, 357-359 (1986).
- A. Blacha, R. Clauberg, H. K. Seitz, and H. Beha, "17 ps Rise-Time Measurement by Photoemission Sampling," *Electron Lett.* 23, 249-250 (1987).

- A. Blacha, R. Clauberg, and H. K. Seitz, "Photoemission Sampling Measurements of a Dispersing Voltage Pulse Travelling on a Transmission Line," J. Appl. Phys. 62, 713-716 (1987).
- A. M. Weiner, P. S. D. Lin, and R. B. Marcus, "Picosecond Temporal Resolution Photoemissive Sampling," Appl. Phys. Lett. 51, 358–360 (1987).
- H. Beha, H. Seitz, A. Blacha, and R. Clauberg, "Photoemission Sampling Technique for High-Speed Integrated Circuit Testing," *Microelectron. Eng.* 7, 351-359 (1987).
- H. Beha and R. Clauberg, "Picosecond Photoemission Probing for High-Speed Integrated Circuits," *Electron Beam Testing Technology*, S. C. J. Garth and W. C. Nixon, Eds., Plenum Press, New York, to be published.
- R. Clauberg and H. Beha, "Laserstrahl-Photoemissions-Testen Ultraschneller Integrierter Schaltkreise," Mikroelektron. 2/1989, 74-77 (1989).
- H. K. Seitz, A. Blacha, R. Clauberg, H. Beha, and J. Feder, "Contactless High-Speed Waveform Measurements on GaAs Integrated Circuits with the Photoemission Sampling Technique," Proceedings of the 1st European Test Conference, Paris, France, April 12–14, 1989, pp. 176–179.
- R. Clauberg, "Microfields in Stroboscopic Voltage Measurements via Electron Emission: I. Response Function of the Potential Energy," J. Appl. Phys. 62, 1553–1559 (1987).
- R. Clauberg, "Microfields in Stroboscopic Voltage Measurements via Electron Emission: II. Effects on Electron Dynamics," J. Appl. Phys. 62, 4017–4023 (1987).
- H. Fujioka, K. Nakamae, and K. Ura, "Analysis of the Transit Time Effect on the Stroboscopic Voltage Contrast in the Scanning Electron Microscope," J. Phys. D 18, 1019–1027 (1985).
- R. Clauberg and A. Blacha, "High Electron Density Effects in Electron Spectroscopies: Consequences for Picosecond Photoemission and Electron Beam Sampling," J. Appl. Phys. 65, 4095–4106 (1989).
- V. S. Fomenko, in *Handbook of Thermionic Properties*, G. V. Samsonov, Ed., Plenum Press, New York, 1966.
- W. F. Krolikowski and W. E. Spicer, "Photoemission Studies of the Noble Metals. I. Copper," *Phys. Rev.* 185, 882–900 (1969).
- P. May, J.-M. Halbout, and G. Chiu, "Picosecond Photoelectron Scanning Electron Microscope for Noncontact Testing of Integrated Circuits," Appl. Phys. Lett. 51, 145-147 (1987).
- P. May, J.-M. Halbout, and G. Chiu, "Noncontact High-Speed Waveform Measurements with the Picosecond Photoelectron Scanning Electron Microscope," *IEEE J. Quantum Electron*. QE-24, 234–239 (1988).
- K. Ura, "Address Error of Electron Beam by Local Electric Field," Optik 58, 281–284 (1981).
- B. Lischke, D. Winkler, and R. Schmitt, "The Limits of High-Speed E-Beam Testing," Microelectron. Eng. 7, 21–39 (1987).
- R. Clauberg, A. Blacha, and H. K. Seitz, "Voltage Detector and Sub-Micrometer Focusing Unit for Photoemission Probing," Rev. Sci. Instrum., to be published.
- M. Born and E. Wolf, Principles of Optics, 6th ed., Pergamon Press, Oxford, U.K., 1987.
- K. Nakamae, H. Fujioka, and K. Ura, "Local Field Effects on Voltage Contrast in the Scanning Electron Microscope," J. Phys. D 14, 1939–1960 (1981).
- L. Reimer and M. Wächter, "Contribution to the Contamination Problem in Transmission Electron Microscopy," *Ultramicroscopy* 3, 169-174 (1978).
- D. W. Ranasinghe, D. J. Machin, and G. Proctor, "Electron Beam Irradiation Effects on MOS-Transistors and Its Significance to E-Beam Testing," *Microelectron. Eng.* 7, 397–403 (1987).
- G. Auvert, "Laser Beam Testing of Finished Integrated Circuits," Microelectron. Eng. 7, 363-370 (1987).
- J. Quincke, F. Dielacher, and K. Goser, "Investigation of Surface-Induced Latch-Up in VLSI CMOS Using the Laser Probe," *Microelectron. Eng.* 7, 371-375 (1987).

 E. Wolfgang, S. Göhrlich, and E. Plies, "Progress in Electron Beam Testing," Proceedings of COMPEURO '89, VLSI and Computer Peripherals, W. E. Pröbster and H. Reiner, Eds., Computer Society of the IEEE, New York, 1989, pp. 5/110– 5/115, and private communications by E. Wolfgang.

Received May 11, 1989; accepted for publication August 11, 1989

Rolf Clauberg IBM Research Division, Zurich Research Laboratory, CH-8803 Rüschlikon, Switzerland. Dr. Clauberg is a Research Staff Member of the Laser Science and Technology Department at the Zurich Research Laboratory. He received his diploma in physics and his Ph.D. in science (Dr. rer. nat.) from the University of Cologne, FRG, in 1980 and 1984, respectively. Both thesis works were performed at the Institut für Festkörperforschung of the Kernforschungsanlage Jülich GmbH in Jülich, FRG, in the field of spin-resolved photoemission, and included work at the ACOstorage ring for synchrotron radiation in Orsay. France, and at the BESSY-storage ring in Berlin. In 1981 Dr. Clauberg was honored with the Max-Auwärter Award for surface science for his theoretical and experimental work on photoemission. He joined the IBM Zurich Research Laboratory in 1985. Dr. Clauberg is a member of the American Physical Society, the German Physical Society (DPG), and the contactless testing committee of the German "Informations-Technische Gesellschaft" (ITG). His current field of interest is optoelectronics, with special emphasis on computational and theoretical analyses.

H. Beha IBM Germany, Plant Sindelfingen, Tuebinger Allee 49, P.O. Box 266, 7032 Sindelfingen 1, Federal Republic of Germany.

Armin Blacha IBM Research Division, Zurich Research Laboratory, CH-8803 Rüschlikon, Switzerland. Dr. Blacha studied physics and mathematics at the Technical University of Braunschweig, FRG, where he received the diploma in physics in 1979. His Ph.D. work was done at the Max-Planck-Institut für Festkörperforschung in Stuttgart. During his studies, he worked in the fields of nuclear magnetic resonance, magnetism, and semiconductor physics (with emphasis on optical properties). In 1985 Dr. Blacha received the Ph.D. from the University of Stuttgart, joining the IBM Zurich Research Laboratory in Rüschlikon. Since 1986, he has been a Research Staff Member at the Zurich Research Laboratory. During the past three years, he has worked on time-resolved photoemission spectroscopy, with special emphasis on applications for electrical probing of high-speed integrated circuits.

Hugo K. Seitz IBM Research Division, Zurich Research Laboratory, CH-8803 Rüschlikon, Switzerland. Mr. Seitz received his M.S. in electrical engineering in 1975 from Syracuse University, New York. He subsequently worked in high-speed electronic device packaging technology, in display and printing technology, and in silicon device research at the IBM Thomas J. Watson Research Center in Yorktown Heights, New York. In 1981 Mr. Seitz transferred to the IBM Zurich Research Laboratory, where he was involved with the design of special electronic instrumentation. In 1985 he joined a small group developing the new contactless testing method.

188